Available online at www.sciencedirect.com
SCIENCE DIRECT®
International Journal of Thermal Sciences 43 (2004) 653–663
International Journal of Thermal Sciences
www.elsevier.com/locate/ijts

Natural convection in a vertical porous slot heated from below and with horizontal concentration gradients ☆

A. Bahloul [a,*], L. Kalla [a], R. Bennacer [b], H. Beji [b], P. Vasseur [a]

[a] *École polytechnique, CP 6079, Succ "Centre Ville", Montréal, Québec H3C 3A7, Canada*
[b] *Lee-Leevan, rue d'Eragny, 95031, Neuville-sur-Oise, France*

Received 25 February 2003; accepted 30 October 2003

Available online 7 January 2004

Abstract

Double-diffusive natural convection in a slender vertical porous enclosure is studied both analytically and numerically. The buoyancy forces that induce the fluid motion result from the imposition of both a vertical temperature gradient and a horizontal solutal gradient. The first part of the study contains an analytical solution valid for stratified flows in enclosures with relatively high aspect ratios. The second part of the study contains a numerical study of the full governing equations that validate the analytical model. Comparison between the numerical and analytical solutions covers the thermal Rayleigh number range $-6 \times 10^2 \leqslant R_T \leqslant 10^4$, the buoyancy range $0 \leqslant N \leqslant 10^3$ and the Lewis number range $10^{-2} \leqslant Le \leqslant 10^2$. In the absence of a horizontal solutal gradient ($N = 0$), the solution takes the form of standard Bénard bifurcation. The asymmetry resulting from the imposition of a small ($N \ll 1$) horizontal solutal gradient is investigated. The existence of multiple solutions, for a given range of the governing parameters, is demonstrated.

1. Introduction

Recent interest in the study of flows with two sources of buoyancy through porous media has been motivated by such diverse engineering problems as electrochemical processes, contaminant transport in saturated soils, food processing, geophysical systems, etc. The growing volume of papers in this field has been recently review by Nield and Bejan [1].

Earlier studies on double-diffusive natural convection in porous media focused on the case of a horizontal layer subject to vertical temperature and concentration gradients. Thus, Nield [2], Tauton et al. [3], Rubin [4] and Poulikakos [5] relied on linear stability theory to investigate the onset of convection for various thermal and solutal boundary conditions. Finite amplitude flow, for this geometrical configuration, was investigated by Rudraiah et al. [6], Brand and Steinberg [7], Murray and Chen [8], Trevisan and Bejan [9] and Chen and Chen [10]. Various flow regimes, steady and unsteady, were identified by these authors. More recently Mamou and Vasseur [11] studied analytically and numerically double diffusive convection in a horizontal cavity under different types of thermal and solutal boundary conditions. The existence of multiple solutions for a given set of the governing parameters, was demonstrated by these authors. Double diffusive convection, in a vertical cavity subject to horizontal temperature gradients, has also be investigated by Trevisan and Bejan [12,13], Alavyoon [14], Alavyoon et al. [15], Goyeau et al. [16], Mamou et al. [17–21] and Charrier Mojtabi et al. [22]. It was demonstrated that, depending on the governing parameters of the problem and on the thermal to solutal buoyancy ratio N, various modes of convection prevail. In particular, in the case of opposing buoyancy forces ($N < 0$), it was observed that there exists an interval of N, depending on the parametric values, in which permanent oscillating flows occur.

The above investigations are dealing with the case of porous layers subject to either horizontal or vertical gradients of heat and mass. In many applications, in industry, oceanography and geophysics, the porous layer is often under the imposition of cross fluxes of heat and mass. Despite this fact, little attention has been dedicated to this type of situation. Kalla et al. [23,24] investigated double diffusive convective within a shallow horizontal porous layer salted from

☆ This work was supported by the Natural Sciences and Engineering Research Council, Canada.
* Corresponding author.
E-mail address: abahloul@polymtl.ca (A. Bahloul).
URL: http://www.polymtl.ca (A. Bahloul, P. Vasseur).

1290-0729/$ – see front matter
doi:10.1016/j.ijthermalsci.2003.10.012

Nomenclature

A_f	aspect ratio of the cavity, $= H'/L'$
C	normalized mass fraction
C_S	dimensionless concentration gradient in y-direction
C_T	dimensionless concentration gradient in y-direction
D	mass diffusivity of species ..... $m^2 \cdot s^{-1}$
g	gravitational acceleration ..... $m \cdot s^{-2}$
H'	height of enclosure ..... m
j'	solute flux per unit area ..... $kg \cdot m^{-2} \cdot s^{-1}$
k	thermal conductivity ..... $W \cdot m^{-1} \cdot K^{-1}$
K	permeability of the porous medium ..... m^2
L'	width of the enclosure ..... m
Le	Lewis number, $= \alpha/D$
N	buoyancy ratio, $= \beta_S \Delta S'/\beta_T \Delta T'$
q'	constant heat flux per unit area ..... $W \cdot m^{-2}$
R_T	thermal Rayleigh number, $= g\beta_T K \Delta T' L'/\alpha\nu$
R_S	solutal Rayleigh number, $= R_T N Le$
S	dimensionless concentration, $= (S' - S'_o)/\Delta S'$
ΔS	dimensionless wall-to-wall concentration difference
S'	concentration of the denser component $kg \cdot m^{-3}$
S'_o	reference concentration at $x' = 0$, $y' = 0$ ..... $kg \cdot m^{-3}$
$\Delta S'$	characteristic concentration, $= j'L'/D$ $kg \cdot m^{-3}$
Sh	Sherwood number, $= 1/\Delta S$, Eq. (31)
t	dimensionless time, $= t'\alpha/\sigma L'^2$
T	dimensionless temperature, $= (T' - T'_o)/\Delta T'$
ΔT^*	related to the intensity of heat transfer, Eq. (30)
T'_o	reference temperature at $x' = 0$, $y' = 0$
$\Delta T'$	characteristic temperature, $= q'L'/k$
u	dimensionless velocity in x-direction, $= u'L'/\alpha$
v	dimensionless velocity in y-direction, $= v'L'/\alpha$
x	dimensionless coordinate axis, $= x'/L'$
y	dimensionless coordinate axis, $= y'/L'$

Greek symbols

α	thermal diffusivity, $= k/(\rho C)_f$ ..... $m^2 \cdot s^{-1}$
β_S	concentration expansion coefficient
β_T	thermal expansion coefficient ..... K^{-1}
ε	normalized porosity of the porous medium, $= \phi/\sigma$
ν	kinematic viscosity of fluid ..... $m^2 \cdot s^{-1}$
μ	dynamic viscosity of the fluid ..... $kg \cdot m^{-1} \cdot s^{-1}$
θ_S	dimensionless h horizontal concentration profile
θ_T	dimensionless h horizontal temperature profile
ρ	density of the fluid ..... $kg \cdot m^{-3}$
$(\rho C)_f$	heat capacity of fluid ..... $J \cdot m^{-3} \cdot K^{-1}$
$(\rho C)_P$	heat capacity of saturated porous medium ..... $J \cdot m^{-3} \cdot K^{-1}$
σ	heat capacity ratio, $= (\rho C)_P/(\rho C)_f$
Ψ	dimensionless stream function, $= \Psi'/\alpha$
Ψ_c	stream function value at the center of the enclosure
ϕ	porosity of the porous medium

Superscript

$'$	dimensional variable

Subscripts

max	maximum value
min	minimum value
o	reference state

the bottom and heated horizontally by an uniform heat flux. The existence of multiple solutions was demonstrated to exist both analytically and numerically. Also, in reference [24], the asymmetry brought by the side heating to the classical Bénard bifurcation was investigated. For supercritical convection the existence of three different solutions is possible, one of these solution being unstable. The case of a cavity, heated and cooled isothermally along vertical walls while concentration gradient is imposed vertically has been considered by Mohamad and Bennacer [25]. Numerical results were obtained for the case of a cavity of aspect ratio two. It was reported that the flow becomes unstable for finite range of solutal-to-thermal buoyancy ratio and it is possible to obtain different solutions in this region. Also, it was found that strong stratified fluid might suppress the thermal convection. Numerical results were also obtained by these authors [26] on the basis of two- and three-dimensional models. It was found that the difference in the rate of heat and mass transfer predicted by the two models was not that significant.

The present paper focuses on the analysis of the flow, the heat and the mass transfers in a tall cavity. A vertical temperature gradient is imposed vertically on the enclosure while uniform mass fluxes are applied along the vertical walls. The layout of the paper is as follows. In the next section the physical system and the mathematical model are introduced. The numerical procedure used to solve the full governing equations is then discussed. This is followed by the derivation of an approximate analytical model, valid for tall cavities. Some results and discussions are presented in the following section. Finally, some conclusions for the present investigation are reported.

2. Problem statement

The physical model and coordinate system are shown in Fig. 1. The geometry under consideration is a two-dimensional vertical enclosure of height H' and width L' filled with saturated porous medium. A vertical heat flux q'

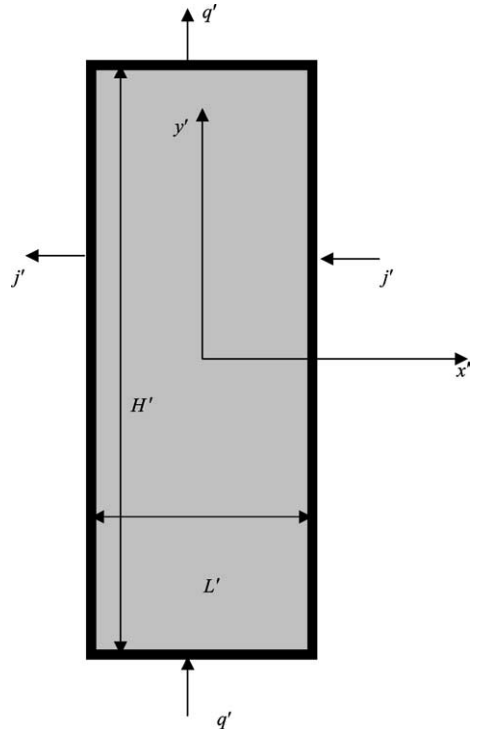

Fig. 1. Schematic of the problem with coordinate system.

is applied on the bottom and top walls. A solute concentration gradient, j', is applied on the two vertical impermeable walls. The fluid is assumed to be incompressible, Newtonian and viscous. The porous medium is considered to be uniform and in local thermal and compositional equilibrium with the fluid. The effect due to viscous dissipation and inertial effects are assumed to be negligible. The thermophysical proprieties of the fluid are assumed to be constant, except density variation in the buoyancy term, which depends linearly on both local temperature and concentration, i.e., Boussinesq approximation is supposed to be valid,

$$\rho = \rho_0\left[1 - \beta_T\left(T' - T'_0\right) - \beta_S\left(S' - S'_0\right)\right] \tag{1}$$

where ρ_0 is the fluid density at temperature T'_0 and concentration S'_0, and β_T and β_S are the thermal and concentration expansion coefficients, respectively. The subscript o refers to conditions at the origin of the coordinate system.

The following dimensionless variables are used

$$\begin{aligned} &(x, y) = \left(x', y'\right)/L', && (u, v) = \left(u', v'\right)L'/\alpha \\ &t = t'\alpha/L'^2\sigma, && T = \left(T' - T'_0\right)/\Delta T' \\ &S = \left(S' - S'_0\right)/\Delta S', && \Delta T' = q'L'/k \\ &\Delta S' = j'L'/D, && \varepsilon = \Phi/\sigma \end{aligned} \tag{2}$$

where t' is the time, k and D the thermal conductivity of the saturated porous medium and the mass averaged diffusivity through the fluid mixture, respectively, $\alpha = k/(\rho C)_f$ the thermal diffusivity of the porous medium, $\sigma = (\rho C)_p/(\rho C)_f$ the saturated porous medium to fluid heat capacity ratio, and Φ the porosity of the porous matrix.

In the following analysis, the stream function formulation is introduced in the mathematical model. In order to satisfy the continuity equation, the stream function Ψ is defined such that $u = \partial\Psi/\partial y$ and $v = -\partial\Psi/\partial x$.

In terms of the above definitions, the dimensionless governing equations expressing conservation of momentum, energy and species are, respectively

$$\nabla^2\Psi = -R_T\frac{\partial}{\partial x}(T + NS) \tag{3}$$

$$\nabla^2 T = u\frac{\partial T}{\partial x} + v\frac{\partial T}{\partial y} + \frac{\partial T}{\partial t} \tag{4}$$

$$\frac{1}{Le}\nabla^2 S = u\frac{\partial S}{\partial x} + v\frac{\partial S}{\partial y} + \varepsilon\frac{\partial S}{\partial t} \tag{5}$$

The dimensionless boundaries, sketched in Fig. 1, are

$$x = \pm\frac{1}{2}, \qquad \Psi = 0, \qquad \frac{\partial T}{\partial x} = 0, \qquad \frac{\partial S}{\partial x} = 1 \tag{6a}$$

$$y = \pm\frac{A_f}{2}, \qquad \Psi = 0, \qquad \frac{\partial T}{\partial y} = -1, \qquad \frac{\partial S}{\partial y} = 0 \tag{6b}$$

The dimensionless parameters that characterize the problem are the aspect ratio of the enclosure $A_f = H'/L'$, the thermal Rayleigh number $R_T = g\beta_T K\Delta T'L'/\alpha\nu$, the solutal to thermal buoyancy ratio $N = \beta_S\Delta S'/\beta_T\Delta T'$, the Lewis number $Le = \alpha/D$ and the normalized porosity ε.

In the above definitions K is the permeability of the porous medium, g the acceleration due to gravity and ν the kinematic viscosity of the fluid.

3. Analytical solution

For a slender cavity ($A_f \gg 1$), it has been demonstrated in the past by several authors (see, for instance, Alavyoon et al. [15] and Mamou et al. [18]) that the governing equations can be significantly simplified by the approximation of the parallel flow. With this approximation $u = 0$ and $v = v(x)$ in the central part of the cavity, i.e., outside the end regions. The approximation allows the following simplifications

$$\Psi = \Psi(x) \tag{7}$$

$$T = C_T y + \theta_T(x) \tag{8}$$

$$S = C_S y + \theta_S(x) \tag{9}$$

where C_T and C_S are constants expressing the gradients of temperature and concentration along the y-direction.

With these approximation the governing equations (3)–(5) reduce to the following expressions

$$\frac{\mathrm{d}^2\Psi}{\mathrm{d}x^2} = -R_T\left(\frac{\mathrm{d}\theta_T}{\mathrm{d}x} + N\frac{\mathrm{d}\theta_S}{\mathrm{d}x}\right) \tag{10}$$

$$\frac{\mathrm{d}^2\theta_T}{\mathrm{d}x^2} = -C_T\frac{\mathrm{d}\Psi}{\mathrm{d}x} \tag{11}$$

$$\frac{\mathrm{d}^2\theta_S}{\mathrm{d}x^2} = -C_S Le\frac{\mathrm{d}\Psi}{\mathrm{d}x} \tag{12}$$

Eqs. (11) and (12), under boundary conditions (6a), can be rewritten as follows

$$\frac{d\theta_T}{dx} = -C_T \Psi \tag{13}$$

$$\frac{d\theta_S}{dx} = -Le\, C_S \Psi + 1 \tag{14}$$

Substituting the above equations into (10) the following governing equation is obtained

$$\frac{d^2\Psi}{dx^2} = A\Psi + B \tag{15}$$

where

$$A = a^2 = R_T C_T + R_S C_S$$
$$B = -R_T N \tag{16}$$

and $R_S = R_T N\, Le$.

The set of ordinary differential equations (13)–(15) can be easily solved to yield a closed form analytical solution. Depending on the sign of A two types of solutions are possible, as discussed, for instance, by Mamou et al. [20]. For the present problem we have:

3.1. Case $A > 0$

By setting $A = a^2$ $(a > 0)$, the solution of Eqs. (13)–(15) satisfying the boundary conditions in the x-direction, gives

$$\Psi(x) = \frac{B}{a^2}\left(\frac{\cosh(ax)}{\cosh(a/2)} - 1\right) \tag{17}$$

$$T(x, y) = C_T(y + D) \tag{18}$$

$$S(x, y) = C_S(y - Le\, D) + x \tag{19}$$

where

$$D = -\frac{B}{a^2}\left[\frac{\sinh(ax)}{a\cosh(a/2)} - x\right]$$

The temperature and concentration gradients in y-direction are determined by imposing zero heat and mass transfer across any transversal section of the cavity (see, for instance, Mamou et al. [17]). In this way, after some algebra, it is found that C_T and C_S can be expressed as

$$C_T = \frac{-1}{1+F}, \qquad C_S = \frac{Le\, G}{1 + Le^2 F} \tag{20a}$$

where

$$F = \int_{-1/2}^{1/2} \Psi^2\, dx, \qquad G = \int_{-1/2}^{1/2} \Psi\, dx \tag{20b}$$

Substituting Eq. (17) into Eq. (20) and performing the resulting integrals it is readily found that

$$F = \frac{B^2}{a^5}\left[\frac{a(\cosh^2(a/2) + 1/2) - 3\cosh(a/2)\sinh(a/2)}{\cosh^2(a/2)}\right] \tag{21}$$

and

$$G = -\frac{B}{a^2}\left[1 - \frac{\tanh(a/2)}{a/2}\right] \tag{22}$$

The above values of C_T and C_S can be combined with the value of $a^2 = R_T C_T + R_S C_S$ to yield

$$a^2(1+F)\left(1 + Le^2 F\right) + R_T F\left(1 + Le^2 F\right) - R_S\, Le\, G(1+F) = 0 \tag{23}$$

The values of C_T and C_S in the stream function and temperature and concentration fields, Eqs. (17)–(19), can be obtained by solving the above transcendental equation for any combination of the controlling parameters R_T, N and Le.

Substituting Eqs. (18) and (19) into Eqs. (8) and (9), it is found that the heat and mass transfers are given, respectively, by

$$\Delta T^* = \frac{a^3}{BC_T[a - 2\tanh(a/2)]} \tag{24}$$

and

$$Sh = \frac{a^3}{BC_S\, Le[2\tanh(a/2) - a] + a^3} \tag{25}$$

3.2. Case $A < 0$

The case $A = -b^2$ $(b > 0)$, is now considered. The resulting equations can be deduced by substituting $a = ib$ in the above solution. Since $\sinh(ib) = i\sin(b)$ and $\cosh(ib) = i\cos(b)$ it follows that resulting solution is similar to that given by Eqs. (17)–(23) with the hyperbolic functions replaced by circular function. For instance, the parameter b can be computed from the following equation

$$b^2(1+F)\left(1 + Le^2 F\right) + R_T F\left(1 + Le^2 F\right) - R_S\, Le\, G(1+F) = 0 \tag{26}$$

In this case F and G are given by:

$$F = \frac{B^2}{b^5}\left[\frac{b(\cos^2(b/2) + 1/2) - 3\cos(b/2)\sin(b/2)}{\cos^2(b/2)}\right] \tag{27}$$

and

$$G = -\frac{B}{b^2}\left[1 - \frac{\tan(b/2)}{b/2}\right] \tag{28}$$

4. Numerical solution

A finite-difference numerical solution technique based on integration over the control volume is used to solve the model equations with appropriate boundary conditions. The hybrid scheme suggested by Patankar [27] was utilized. This scheme employs the upwind method only when the coefficient matrix becomes negative due to a large value of the velocity in the convection term. All other points are approximated by central differences. The application of the method to the solution of natural convection problems has been discussed in details in the past and does not need to be repeated here.

In order to improve the resolution of dependent variables a non-uniform grid was used. The non-uniform grid has denser clustering near the wall boundaries. Grid independency of the results was established by employing different size meshes, ranging in size from 40×120 to 60×180. The results indicated a maximum relative difference of about 1.5% in the value of the maximum stream function $\Psi_{\max}$. Additionally, the relative difference between both grids for the vertical velocity profile, at the center of the cavity, is less than 1.2%. Thus a 60×180 grid was used for all the results reported here.

To ensure convergence of the numerical algorithm the following criteria is applied to all dependent variables over the solution domain

$$\sum_i \sum_j \frac{|\phi_{i,j}^{n+1} - \phi_{i,j}^{n}|}{\sum_i \sum_j |\phi_{i,j}^{n+1}|} \leqslant 10^{-9} \tag{29}$$

where ϕ represent a dependent variable, the indexes i, j indicated a grid point and the index n the current iteration.

Typical numerical results are presented in Fig. 2 for $R_T = 400$, $Le = 2$, $N = 0.1$ and $A_f = 8$. On the graph streamlines, isotherms and isoconcentrates are presented in Fig. 2(a) from left to right. From theses results, it is clear that for a tall cavity ($A_f \gg 1$) the flow in the core region of the enclosure is essentially parallel while the temperature and concentration are linearly stratified in the vertical direction. The analytical solution, developed in this study relies on these observations. Fig. 2(b) shows the streamfunction, temperature and concentration distributions in the horizontal mid-plane ($y = 0$). The agreement with the numerical and the analytical results is observed to be excellent. Numerical tests have been performed to determine the minimum aspect ratio above which the flow can be assumed to be parallel. In the range of the parameters considered here it was found that the numerical results can be considered independent of the aspect ratio when $A_f \geqslant 6$. For this reason most of the results presented in this investigation were obtained for $A_f = 8$.

In the present notation, the heat and the mass transfers within the cavity are given respectively by the flowing expressions

$$\Delta T^* = \frac{q'}{k\overline{\Delta T'}/L'} = \frac{1}{\Delta T} \tag{30}$$

and

$$Sh = \frac{j'}{D\overline{\Delta S'}/L'} = \frac{1}{\Delta S} \tag{31}$$

where

$$\overline{\Delta T'} = T'(0, 1/2) - T'(0, -1/2) \quad \text{and}$$
$$\overline{\Delta S'} = S'(0, 1/2) - S'(0, -1/2)$$

are the temperature and concentration differences between the right and left walls of the enclosure at the position $y = 0$.

It is noted that the present analytical solution is not valid in the vicinity of the thermally active boundaries. Thus, it is not possible to predict analytically the Nusselt number in terms of the temperature differences between the horizontal walls. For this reason, the temperature difference ΔT^*, between the vertical walls, is used here as an indication of the intensity of the heat transfer within the enclosure.

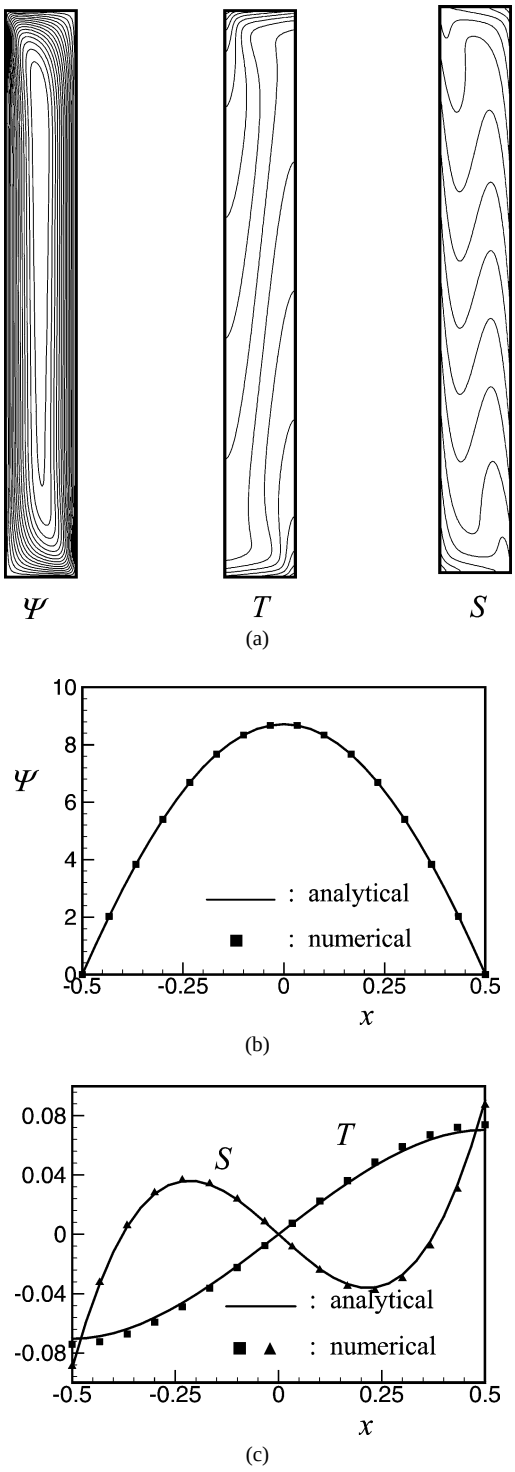

Fig. 2. Numerical results for $R_T = 400$, $Le = 2$, $N = 0.1$ and $A_f = 8$; (a) Contour lines of streamfunction, temperature and concentration; (b) distribution of streamfunction, (c) temperature and concentration in the horizontal mid-plane, $\Psi_c = 8.714$, $\Delta T^* = 7.094$, $Sh = 5.537$.

5. Results and discusion

In the present section a comparison is made between the analytical model based on the parallel flow approximation and the numerical solution of the full governing equations described early. As discussed above, the present problem is governed by five dimensionless parameters, namely R_T, Le, N, A_f and ε. In the following discussion, it is assumed that the normalized porosity of the porous medium is $\varepsilon = 1$. Also, the analytical results predicted by the present model are more accurate at large value of A_f ($A_f \gg 1$).

5.1. Convection induced solely by vertical gradients of heat ($N \ll 1$)

The case of convection in a vertical layer heated from the bottom by a constant heat flux corresponds to the limit $N \ll 1$. For this situation, it can be deduced from the equations corresponding to the case $A < 0$ that

$$\Psi^n = \frac{P^n R_T}{n^2\pi^2}\cos(n\pi x) \tag{32a}$$

$$T^n = -\frac{n^2\pi^2}{R_T}y + \frac{P^n R_T}{n\pi}\sin(n\pi x) \tag{32b}$$

$$\Delta T^* = \frac{2n\pi}{p^n R_T}(-1)^n \tag{32c}$$

where

$$P^n = \pm\frac{n\pi}{R_T}\sqrt{2\left(R_T - n^2\pi^2\right)} \tag{32d}$$

and $n = 1, 3, 5, \ldots$ corresponds to the number of cells. Only the first mode $n = 1$ is unicellular. The above equations are similar to those reported by Sen et al. [28] while studying the occurrence of multiple solutions in an inclined tall cavity heated from below by a constant heat flux.

Fig. 3(a) shows the bifurcation diagram for Ψ_C as a function of thermal Rayleigh number R_T. The particular case considered here corresponds to a classical Rayleigh–Bénard situation for which a conductive state ($T = -y$, $\Psi = 0$) exists, up to a critical Rayleigh number R_{TC} above which convection occurs. From Eq. (32d) it is seen that convection is possible for $R_{TC} > n^2\pi^2$, such that the lowest R_{TC} at which convective motion occurs is given by the unicellular flow for which $R_{TC} = \pi^2$. A similar result has been predicted in the past by Sen et al. [28] on the basis of the linear stability analysis.

The prediction of the onset of convection is correctly predicted by the parallel flow approximation due to fact that the onset of motion, within a vertical layer heated from below by a constant heat flow, occurs at zero wave number. From Fig. 3(a) it is observed that, above the supercritical Rayleigh number $R_{TC} = \pi^2$, the resulting unicellular flow can rotate indifferently clockwise or counterclockwise in agreement with the plus or minus sign in front of Eq. (32d). The analytical solution, represented by a solid line, is seen to be in excellent agreement with the numerical solution of the full governing equations, depicted by black dots. The effect of R_T on ΔT^* is presented in Fig. 3(b). Here again, a good agreement between the analytical and numerical results, is observed.

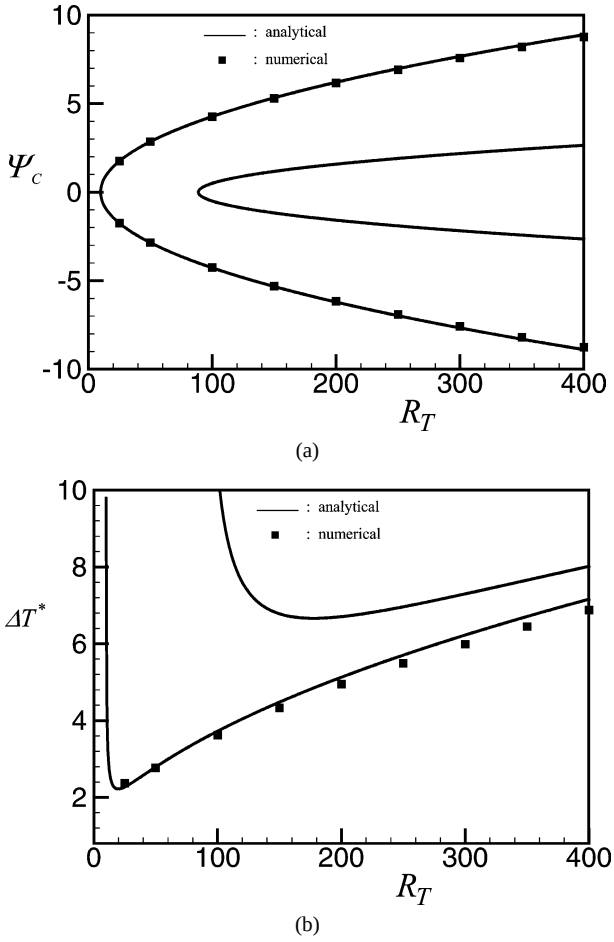

Fig. 3. Bifurcation diagram for $N \ll 1$: (a) Ψ_c versus R_T; and (b) ΔT^* versus R_T.

According to the analytical model depicted above multicellular convection, consisting in n cells in the x-direction, is possible (in Fig. 3, only the multicellular mode $n = 3$ is represented). However, it has not been possible to confirm numerically, the existence of these modes. It is then believed that these modes are unstable.

5.2. Convection induced solely by horizontal gradients of solute ($N \gg 1$)

The case of convection resulting only from the imposition of constant fluxes of concentration, j', on the vertical walls of the cavity, can be deduced from the present theory. This situation corresponds to the limit $N \gg 1$, for which it can be demonstrated from Eqs. (17)–(23) that

$$\overline{\Psi} = \frac{R_S}{a^2}\left(1 - \frac{\cosh(ax)}{\cosh(a/2)}\right) \tag{33a}$$

$$S(x, y) = C_S(y + D) + x \tag{33b}$$

and

$$Sh = \frac{a^3}{R_S C_S[2\tanh(a/2) - a] + a^3} \tag{33c}$$

where

$$a^2 = R_S C_S$$
$$D = -\frac{Rs}{a^2}\left[\frac{\sinh(ax)}{a\cosh(a/2)} - x\right] \tag{33d}$$
$$\overline{\Psi} = \Psi/Le$$

Furthermore, in the boundary layer regime, for which $R_S \gg 1$, it is readily found from Eqs. (33) that

$$\overline{\Psi}_c \approx \sqrt{a} \tag{34a}$$

$$Sh \approx a/2 \tag{34b}$$

where $a = R_S^{2/5}$.

Fig. 4(a) and (b) show, the evolution of Ψ_C and Sh with the solutal Rayleigh number $R_S = R_T N Le$. The variable $\overline{\Psi} = Le\,\Psi$, correspond to a streamfunction normalized with respect with the mass diffusivity of species D. With this renormalization, the evolution of $\overline{\Psi}_C$ versus R_S can be represented by a single curve, independently of Le. Due to the solutal boundary conditions considered here, the resulting unicellular convective cell rotates in a anticlockwise direction ($\overline{\Psi}_C > 0$). The boundary layer regime, valid approximately for $R_S \geqslant 10^3$, is also described as a dashed line in the graph. Here again it is observed that the analytical solution, based on the parallel flow hypothesis, agrees well with the numerical results.

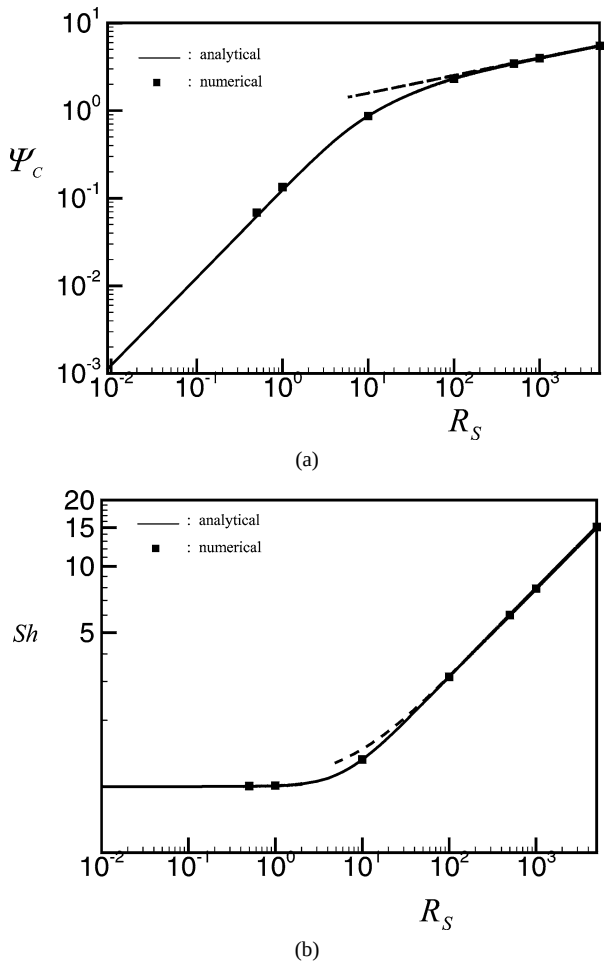

Fig. 4. Effect of solutal Rayleigh number R_S for $R_T \ll 1$ on (a) Ψ_C; and (b) Sh.

5.3. Convection induced by cross gradients of heat and solute

In this section natural convection is considered for intermediate values of N for which the flows result from the imposition of cross temperature and concentration gradients.

Fig. 5(a)–(c) illustrate the effect of the imposition on the vertical walls of a small horizontal solutal gradient ($N = 0.01$, 0.5 and 1) on the magnitude of the stream function Ψ_C and the heat and mass transfers, ΔT^* and Sh, at the center of the cavity as a function of R_T for $Le = 10$. As discussed in Fig. 3(a), in the absence of solutal buoyancy forces ($N = 0$), the resulting flow pattern is induced solely by the vertical thermal gradient imposed on the horizontal wall. For this situation, convection is possible only when the Rayleigh number is above a critical value $R_{TC} > \pi^2$ and the resulting unicellular flow can rotate indifferently clockwise or counterclockwise. The imposition of a horizontal solutal gradient ($N \neq 0$) changes considerably this situation. Thus, it is observed from Fig. 5(a) that convection is now possible for any value of the thermal Rayleigh number. The resulting flow circulation is counterclockwise ($\Psi_c > 0$) in agreement the solutal boundary conditions of Fig. 1. These flows, which numerically can develop from the rest state ($\Psi = 0$) as initial conditions, are referred as "natural flows". However, as it can be observed from Fig. 5(a), the clockwise circulation existing for $N = 0$ is also possible if N is sufficiently small and R_T is above a critical value which depends upon the values of N and Le. The flows, which rotate in direction opposite to the buoyancy forces imposed by the horizontal solutal gradient, are called "antinatural". These type of flows have been discussed in details in reference [27]. These two different solutions are illustrated in Fig. 6 which show the contour lines of streamfunction, temperature and concentration for the natural (Fig. 6(a)) and antinatural (Fig. 6(b)) stable flows that coexist for $R_T = 100$, $N = 0.01$, $Le = 10$ and $A_f = 8$. Numerically, the antinatural flows can be reached only by imposing an impulsing flow pattern rotating in the appropriate direction as an initial condition. Once an antinatural state could have been obtained, for a given value of R_T, it can be used as initial conditions to run another antinatural state for a new R_T. It is noticed that for a given value of N there is a critical value of R_T for the existence of antinatural states. The value of R_{Tc}, predicted by the analytical model, is presented in Fig. 5(d) as a function of N. Thus, for instance, for $N = 0.5$ and $Le = 10$ antinatural flows are possible only in the range of $13 \leqslant R_T \leqslant 360$. In Fig. 5, the analytical solution for antinatural

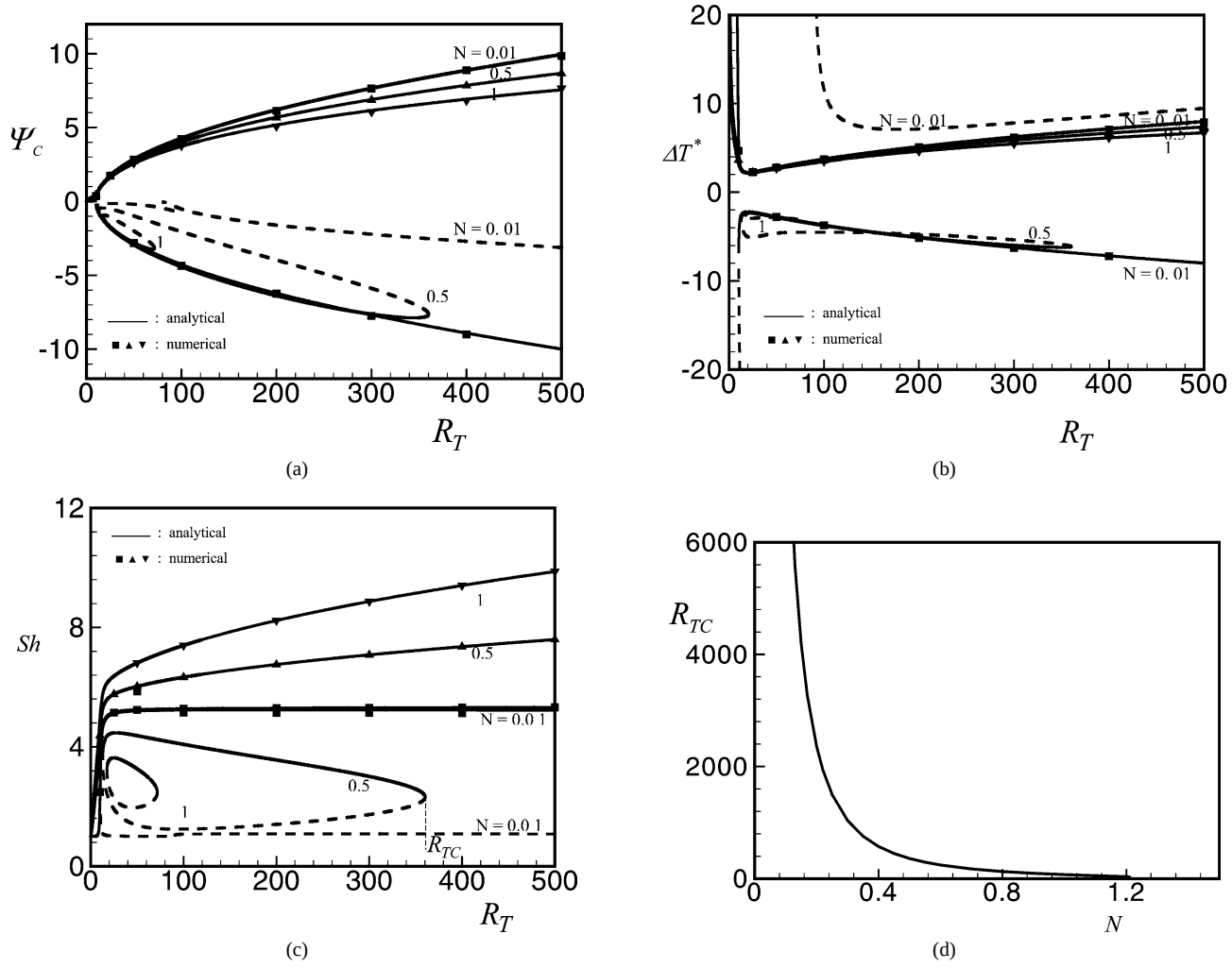

Fig. 5. Effect of thermal Rayleigh number R_T and buoyancy ratio N for $Le = 10$ on (a) Ψ_C; (b) ΔT^*; (c) Sh; and (d) Critical Rayleigh number R_{TC} as a function of N for the existence of antinatural flows.

flows is represented by a solid line, corresponds to an unicellular flow pattern, while the dashed line corresponds to a three cellular flows pattern. Numerical confirmation of the one cell antinatural mode has been obtained for very small values of N. However, it has not been possible to simulate numerically the three cells mode predicted by the analytical model, which is thus believed to be unstable. Whenever a numerical solution could have been obtained it is observed from Fig. 5(a)–(c) that this latter is in general in very good agreement with the analytical model resulting from the parallel flow approximation.

Fig. 7 shows the effect of R_T on the magnitude of Ψ_C for $Le = 10$, $R_S = 10$ and $-600 \leqslant R_T \leqslant 600$. In this graph the case $R_T = 0$ corresponds to convection induced by a destabilizing horizontal solutal gradient in the absence of thermal effects. For $R_T \geqslant 0$ both the thermal and the solutal effects contribute to promote the intensity of convection such that Ψ_C increases with R_T. However, the case of $R_T \leqslant 0$ corresponds to a cavity heated from the top and cooled from the below. The resulting thermal vertical gradient is now stabilizing the system such that $\Psi_C \to 0$ as the value of R_T is increased. An exellent agreement between the analytical on the numerical model is observed in Fig. 7 even for the very low values of Ψ_C obtained for the negative values of R_T.

Fig. 8(a) illustrates the effect of the buoyancy ration N on Ψ_C for $Le = 10$ and various values of R_T. As discussed earlier, for $N = 0$, the flow circulation induced solely by the vertical thermal gradient rotates indifferently clockwise or counterclockwise. Thus, for sufficiently low values of N, it is observed Fig. 8(a) that for a given value of R_T the strength of the anticlockwise natural flow ($\Psi_C > 0$) is approximately the same as that of the clockwise natural flow ($\Psi_C < 0$). Naturally, the natural flow exists for any value of the buoyancy ratio N. As the value of N is made larger the flow pattern is progressively more and more driven by the solutal gradients. Thus, the value of Ψ_C increases with N, i.e., with $R_S = R_T N\, Le$, to reach the boundary layer regime depicted by the dashed lines in the graph. Numerical confirmation of the natural flow circulation is obtained for the range of parameters considered here. On the other hand, it is observed from Fig. 7(a) that, as expected, the antinatural flow circulation is possible only if the value

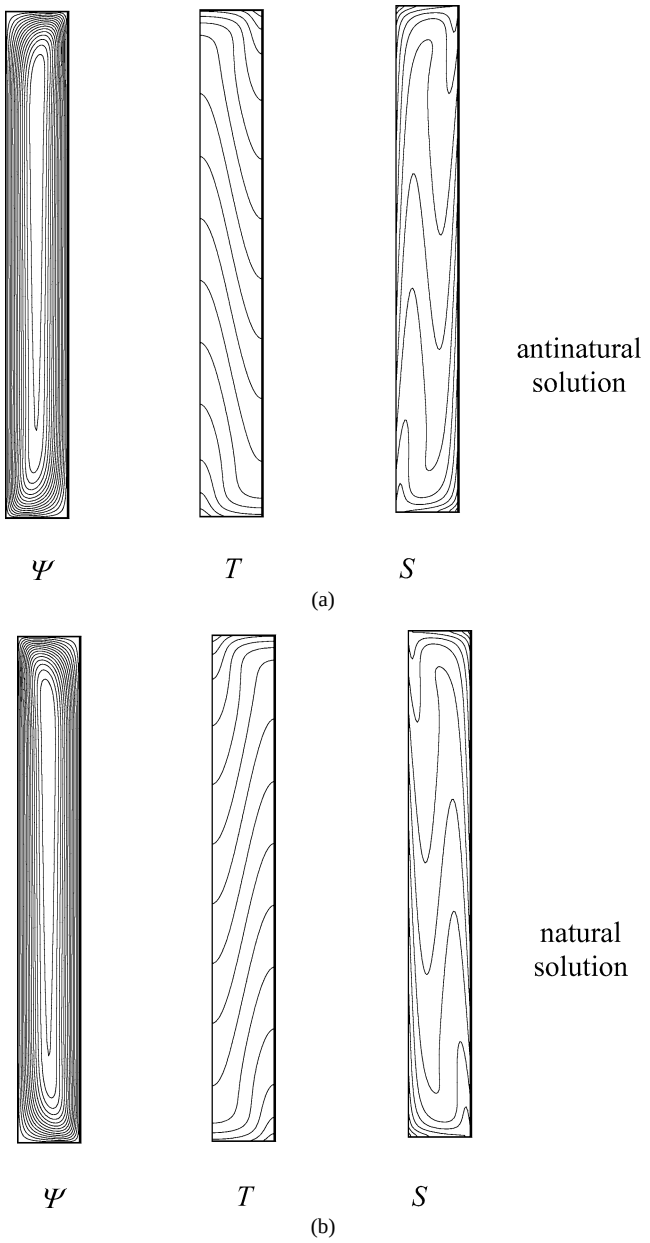

Fig. 6. Contour lines of streamfunction, temperature and concentration for $Le = 10$, $N = 0.01$ and $R_T = 100$: (a) antinatural solution; and (b) natural solution.

of N is below a critical value N_c which depends upon R_T. Thus $N_c = 1.11$ for $R_T = 50$ and $N_c = 0.43$ for $R_T = 500$. The value of N_c, predicted by the analytical model, is presented in Fig. 8(b) as a function of R_T. Numerical confirmation of the antinatural flow is depicted in Fig. 8(a). It was found impossible to obtain numerical results in the vicinity of the turning point N_c. In fact, the numerical results obtained for values of N above those indicated on the graph were found to bifurcate towards the natural flow solution.

The effect of the Lewis number Le on the magnitude of the stream function at the center of the cavity Ψ_C is presented in Fig. 9(a) as a function of the buoyancy

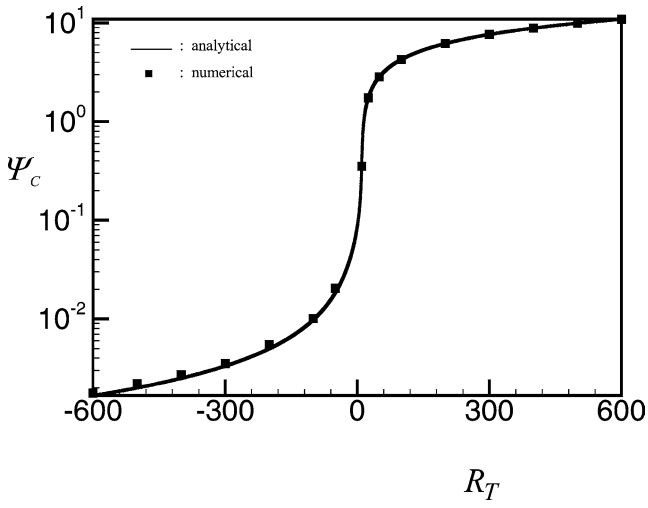

Fig. 7. Effect of thermal Rayleigh number R_T (case of a layer heated from the top and bottom) for $Le = 10$ and $R_S = 10$ on Ψ_C.

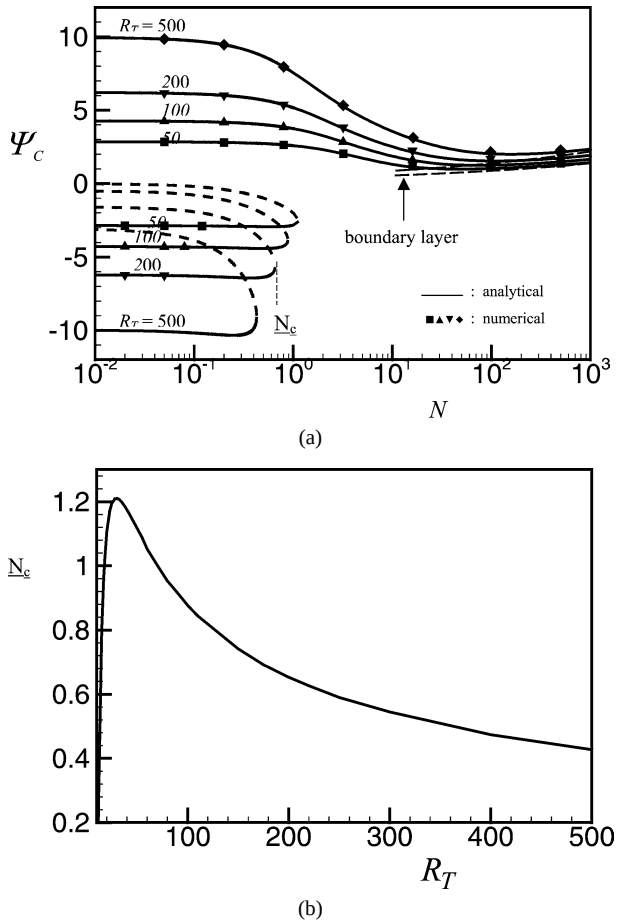

Fig. 8. (a) Flow intensity Ψ_C as a function of buoyancy ratio N and thermal Rayleigh number R_T for $Le = 10$ and (b) critical buoyancy ratio N_C as a function of R_T for the existence of antinatural flows.

ratio N. When N is sufficiently small the flow circulation is driven mostly by the thermal effect and the results are independent of the Lewis effect. For large values of N the flow is then driven by the solutal buoyancy forces and Ψ_C

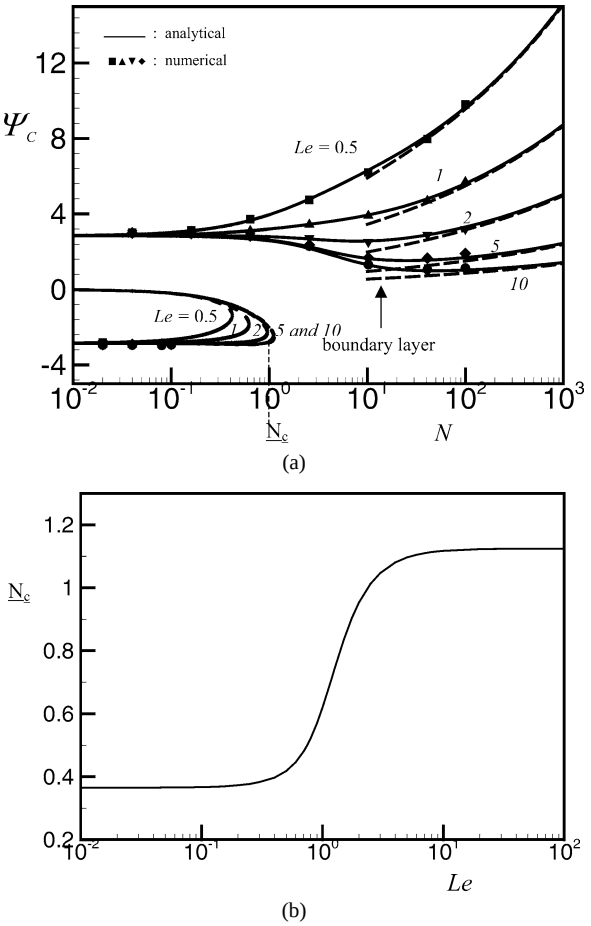

Fig. 9. (a) Flow intensity Ψ_C as a function of buoyancy ratio N and Lewis number Le for $R_T = 50$ and (b) critical buoyancy ratio N_C as a function of Le for the existence of antinatural flows.

is observed to depend strongly upon the value of Le. This is due to the fact that Ψ_C is normalized with respect to the thermal diffusivity α. However, as discussed in Fig. 4 upon normalizing Ψ_C with respect to the mass diffusivity D (i.e., $\overline{\Psi}_C$), the results would be independent of Le. It is also observed from Fig. 9(a) that N_c, the maximum value of N for the existence of antinatural flows, depends upon the value of Le. This is illustrated in Fig. 9(b) which shows the variation of N_c with Le as predicted by the analytical model for $R_T = 50$. It is seen that $N_C \to 0.38$ as $Le \to 0$ while $N_C \to 1.1$ as $Le \to \infty$. The transition between these two asymptotic values occurs in the range $0.1 \leqslant Le \leqslant 10$.

6. Summary

A study is conducted to investigate the patterns and characteristics associated with the double diffusion convection in a tall vertical cavity heated from the below and salted from the sides. The effects of the controlling parameters, including the thermal Rayleigh number, Lewis number and buoyancy ratio on the present problem is investigated. The major results can be summarized as follows:

(i) The numerical solution of the full governing equations indicate that for $A_f \gg 1$ the flow is parallel in the central part of the enclosure while the vertical temperature and concentration fields are linearly stratified.
(ii) An analytical solution of the steady state equations, based on the parallel flow approximation, leads to relatively simple solutions. Closed form expressions are obtained in the two extreme cases of heat transfer ($N = 0$) and mass transfer ($N \to \infty$) driven flows.
(iii) The existence of multiple solutions, for a given set of the governing parameters has been demonstrated both analytically and numerically for the case of small values of the buoyancy ratio N. Thus depending upon the initial conditions used to start the numerical code "natural flows" and "antinatural flows" can be observed in the system.

References

[1] D.A. Nield, A. Bejan, Convection in Porous Media, Springer, Berlin, 1999.
[2] D.A. Nield, Onset of thermohaline convection in a porous medium, Water Resour. Res. 4 (1968) 553–560.
[3] J.W. Tauton, E.B. Lightfoot, T. Green, Thermohaline instability and salt fingers in a porous medium, J. Phys. Fluids 15 (1972) 748–753.
[4] H.Y. Rubin, Effect of solute dispertion on thermal convection in a porous medium layer, Water Resour. Res. 9 (1973) 968–974.
[5] D. Poulikakos, Double-diffusive convection in a horizontally sparsely packed porous layer, Internat. Comm. Heat Mass Transfer 13 (1986) 587–598.
[6] N. Rudraiah, P.K. Shrimani, R. Friedrich, Finite amplitude convection in a two component fluid saturated porous layer, Internat. J. Heat Mass Transfer 25 (1982) 715–722.
[7] H. Brand, V. Steinberg, Nonlinear effect in the convective instability of a binary mixture in a porous medium near threshold, Phys. Lett. A 93 (1983) 333–336.
[8] B.T. Murray, C.F. Chen, Double diffusive convection in a porous medium, J. Fluid Mech. 201 (1989) 147–166.
[9] O.V. Trevisan, A. Bejan, Mass and heat transfer by high Rayleigh number convection in a porous medium heated from below, Internat. J. Heat Mass Transfer 30 (1987) 2341–2356.
[10] F. Chen, C.F. Chen, Double diffusive fingering in a porous medium, Internat. J. Heat Mass Transfer 36 (1993) 793–807.
[11] M. Mamou, P. Vasseur, Thermosolutal bifurcation phenomena in porous enclosures subject to vertical temperature and concentration gradients, J. Fluid Mech. 395 (1999) 61–87.
[12] O.V. Trevisan, A. Bejan, Natural convection with combined heat mass transfer buoyancy effects in a porous medium, Internat. J. Heat Mass Transfer 28 (1985) 1597–1611.
[13] O.V. Trevisan, A. Bejan, Mass and heat transfer by natural convection in a vertical slot filled with porous medium, Internat. J. Heat Mass Transfer 29 (1986) 403–415.
[14] F. Alavyoon, On natural convection in a vertical porous enclosure due to prescribed fluxes of heat and mass at the vertical boundaries, Internat. J. Heat Mass Transfer 36 (1993) 2479–2498.
[15] F. Alavyoon, Y. Masuda, S. Kimura, On natural convection in a vertical porous enclosure due to opposing fluxes of heat and mass prescribed at the vertical walls, Internat. J. Heat Mass Transfer 37 (1994) 195–206.

[16] B. Goyeau, J.P. Songbe, D. Gobin, Numericaly study of double-diffusive convection in a porous cavity using Darcy–Brinkman, Internat. J. Heat Mass Transfer 39 (1996) 1363–1378.
[17] M. Mamou, P. Vasseur, E. Bilgen, Multiple solutions for double-diffusive convection in a vertical porous enclosure, Internat. J. Heat Mass Transfer 38 (1995) 1787–1798.
[18] M. Mamou, P. Vasseur, E. Bilgen, D. Gobin, Double-diffusive convection in an inclined slot filled with porous medium, European J. Mech. B Fluids 14 (1995) 629–652.
[19] M. Mamou, M. Hasnaoui, A. Amahmid, P. Vasseur, Stability of double-diffusive convection in a vertical Brinkman porous enclosure, Internat. Comm. Heat Mass Transfer 25 (1998) 491–500.
[20] M. Mamou, P. Vasseur, E. Bilgen, A Galerkin finite element study of the onset of double-diffusive convection in an inclined porous enclosure, Internat. J. Heat Mass Transfer 41 (1998) 1513–1529.
[21] M. Mamou, P. Vasseur, E. Bilgen, Double-diffusive convection instability in a vertical porous enclosure, J. Fluid Mech. 368 (1998) 263–289.
[22] M.C. Charrier-Mojtabi, M. Karimi-Fard, M. Azaiez, A. Mojtabi, Onset of double-diffusive convection regime in a rectangular porous cavity, J. Porous Media 1 (1998) 107–121.
[23] L. Kalla, P. Vasseur, R. Benacer, H. Beji, R. Duval, Double-diffusive convection within a horizontal porous layer salted from the bottom and heated horizontally, Internat. Comm. J. Heat Mass Transfer 28 (2001) 1–10.
[24] L. Kalla, M. Mamou, P. Vasseur, L. Robillard, Multiple solutions for double-diffusive convection in a shallow porous cavity with vertical fluxes of heat and mass, Internat. J. Heat Mass Transfer 44 (2001) 4493–4504.
[25] A. Mohamad, R. Bennacer, Natural convection in a confined saturated porous medium with horizontal temperature and vertical solutal gradients, Internat. J. Therm. Sci. 40 (2001) 82–93.
[26] A. Mohamad, R. Bennacer, Double diffusion natural convection in an enclosure filled with saturated porous medium subjected to cross gradient stably stratified, Internat. J. Heat Mass Transfer 45 (2002) 3725–3741.
[27] A. Patankar, Numerical Heat Transfer and Fluid Flow: Computational Methods in Mechanics and Thermal Science, Hemisphere, Washington, DC, 1980.
[28] Mihir Sen, P. Vasseur, L. Robillard, Multiple steady states for unicellular natural convection in an inclined porous layer, Internat. J. Heat Mass Transfer 30 (1987) 2097–2113.